Cell

Proteolysis inside the Membrane Is a Rate-Governed Reaction Not Driven by Substrate Affinity

Seth W. Dickey,[1] Rosanna P. Baker,[1] Sangwoo Cho,[1] and Siniša Urban[1,*]
[1]Howard Hughes Medical Institute, Department of Molecular Biology & Genetics, Johns Hopkins University School of Medicine, Room 507 PCTB, 725 North Wolfe Street, Baltimore, MD 21205, USA
*Correspondence: surban@jhmi.edu
http://dx.doi.org/10.1016/j.cell.2013.10.053

SUMMARY

Enzymatic cleavage of transmembrane anchors to release proteins from the membrane controls diverse signaling pathways and is implicated in more than a dozen diseases. How catalysis works within the viscous, water-excluding, two-dimensional membrane is unknown. We developed an inducible reconstitution system to interrogate rhomboid proteolysis quantitatively within the membrane in real time. Remarkably, rhomboid proteases displayed no physiological affinity for substrates (K_d ~190 μM/0.1 mol%). Instead, ~10,000-fold differences in proteolytic efficiency with substrate mutants and diverse rhomboid proteases were reflected in k_{cat} values alone. Analysis of gate-open mutant and solvent isotope effects revealed that substrate gating, not hydrolysis, is rate limiting. Ultimately, a single proteolytic event within the membrane normally takes minutes. Rhomboid intramembrane proteolysis is thus a slow, kinetically controlled reaction not driven by transmembrane protein-protein affinity. These properties are unlike those of other studied proteases or membrane proteins but are strikingly reminiscent of one subset of DNA-repair enzymes, raising important mechanistic and drug-design implications.

INTRODUCTION

All proteins in a living cell are eventually cleaved by proteases (Doucet et al., 2008; López-Otín and Bond, 2008). The purpose of these enzymatic events ranges from shredding damaged proteins that might otherwise harm the cell, to sculpting signal precursors to initiate cell communication (López-Otín and Bond, 2008). Aside from controlling essential processes in all forms of life, protease inhibition has proven to be a particularly effective therapeutic strategy, especially in hypertension and antiviral treatment (Drag and Salvesen, 2010).

Ultimately, deciphering how a protease shapes the signaling characteristics of healthy cells, or targeting it for therapeutic intervention in disease, requires a sophisticated understanding of its enzymatic properties. Kinetic dissection of protease catalysis has been key in revealing these properties (Huntington, 2012; Perona and Craik, 1997; Timmer et al., 2009). Coupled with structural analyses, these studies have established that both cytosolic and extracellular proteases are designed to bind their substrates specifically at discrete sites, with affinity reflected in the Michaelis constant (K_M), and endowed with catalytic residues that function in rate enhancement, reflected in the turnover number (k_{cat}). The catalytic efficiency of a protease is the quotient of these two parameters and typically ranges from 10^4 to 10^7 $M^{-1}s^{-1}$ (10^8 reflects enzymes whose activity is limited by diffusion).

Intramembrane proteases, in contrast to these well-studied soluble proteases, are a more recently discovered class of extraordinary enzymes that evolved independently to catalyze hydrolysis immersed within the membrane (De Strooper and Annaert, 2010; Fluhrer et al., 2009; Makinoshima and Glickman, 2006; Urban and Dickey, 2011; Wolfe, 2009). Despite this complexity, there is significant incentive for understanding how proteolysis is accomplished within these constraints because intramembrane proteases hold great promise for developing therapies: rhomboid proteases are implicated in Parkinson's disease and parasite invasion (Urban and Dickey, 2011); γ-secretase in Alzheimer's disease and leukemia (De Strooper and Annaert, 2010; Wolfe, 2009); signal peptide peptidases in immunity and hepatitis C virus assembly (Fluhrer et al., 2009); and site-2 proteases in the virulence of some of the world's deadliest bacterial and fungal pathogens (Makinoshima and Glickman, 2006; Urban, 2009).

Major insights into the molecular architecture of these remarkable enzymes have been gained from a series of high-resolution intramembrane protease crystal structures of prokaryotic orthologs (Li et al., 2013; Wolfe, 2009), as led by analyses of the *Escherichia coli* rhomboid protease GlpG (summarized in Urban, 2010). In contrast, analysis of catalysis within the membrane in quantitative terms has not been achieved with any intramembrane protease, making it difficult to decipher their functional properties. Current models are based largely on extrapolations from soluble proteases, which evolved independently and are different. In fact, the membrane is a fundamentally unusual setting for proteolysis: chemically, the membrane is viscous and excludes water, which is both essential for

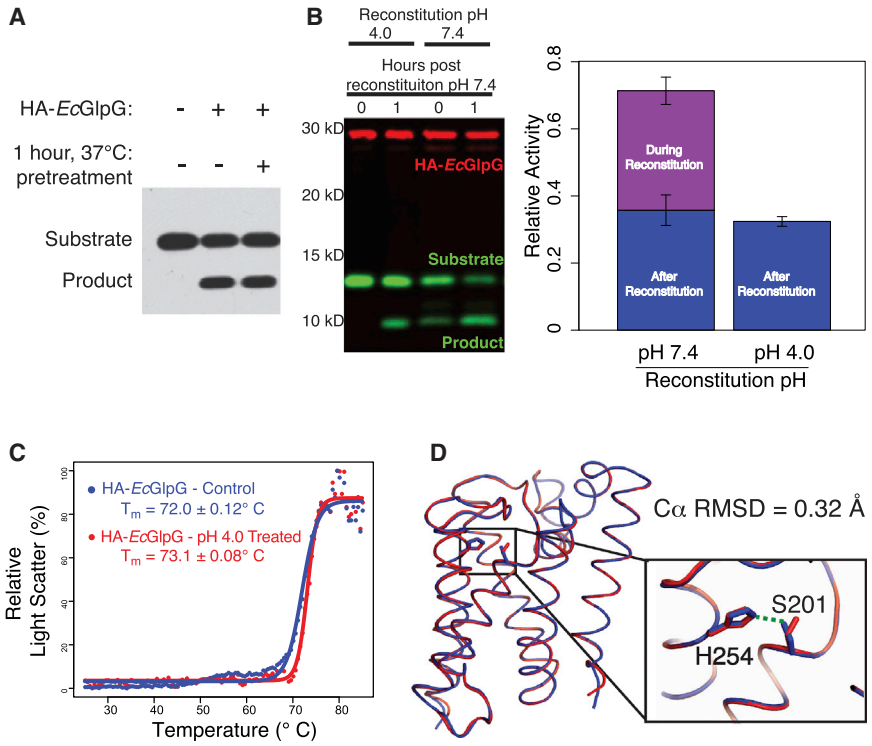

Figure 1. An Inducible Coreconstitution System for Membrane Enzyme Analysis

(A) HA-tagged GlpG (HA-*Ec*GlpG) preincubated for 1 hr at 37°C retained full activity against the substrate APP-Spi7-Flag (shown is an anti-Flag western).

(B) HA-*Ec*GlpG was inactive during the reconstitution with APP-Spi7-Flag at pH 4 but active when reconstituted at pH 7.4 (t = 0 reaction times). Activity was restored upon neutralization to pH 7.4 (see 1 hr reaction time). Shown is a two-color western, and quantification (graph, mean ± SD) revealing the amount of protease activity in proteoliposomes was indistinguishable whether the protease was subjected to pH shift or not.

(C) Thermostability of HA-*Ec*GlpG without and after pretreatment in pH 4 buffer was examined by heating from 25°C to 85°C and monitoring differential static light scattering every 0.5°C.

(D) X-ray crystal structure compares ΔN-*Ec*GlpG at low (red) and neutral (blue) pH. Note that although the overall conformation is indistinguishable (Cα rmsd = 0.32 Å), at low pH, the catalytic serine 201 side chain was no longer hydrogen bonded to the histidine base (inset), rendering the enzyme catalytically inactive.

See Table S1 for structural parameters.

proteolysis and affects how proteins interact. Spatially, proteins in a membrane exist in a two-dimensional plane and are orientationally confined relative to each other. Although techniques for studying proteins inside the membrane are scarce, understanding the consequences of this environment, and how intramembrane proteases function within it, requires interrogating the kinetics of proteolysis within its natural membrane setting.

We have overcome multiple inherent limitations to develop an "inducible" membrane reconstitution system for the quantitative analysis of rhomboid proteolysis occurring within the membrane and in real time. The results reveal that rhomboid proteolysis is a slow reaction that is not driven by affinity of enzyme for substrate. Instead, these insights suggest a different mode of action for this ancient and widespread family of enzymes.

RESULTS

Development of an Inducible Coreconstitution System

In order to study kinetics of proteolysis directly within the membrane, we faced three obstacles that are inherent to GlpG and substrate both being transmembrane proteins. First, although membrane proteins are prone to aggregation in vitro, an important requirement for kinetic analysis is that enzyme concentration does not change during the course of the reaction. We evaluated this concern and found no loss in activity upon preincubating *E. coli* GlpG at 37°C for 1 hr prior to initiating the reaction (Figure 1A), revealing that GlpG enzyme preparations are robust for kinetic analysis.

The greatest challenge to kinetic analysis of proteolysis within membranes is that cleavage already begins during the lengthy procedure to reconstitute protease and substrate into the membrane (Osenkowski et al., 2008). To overcome this obstacle, we developed a rapid and reliable coreconstitution method in which proteolytic activity can be switched off and on. We reasoned that coreconstituting at lower pH would protonate the catalytic histidine, rendering it catalytically inactive. Then, after collecting the proteoliposomes by ultracentrifugation, we planned to initiate the reaction by raising the pH to the physiological 7.4. Under these conditions, we detected no proteolysis during the lowered pH coreconstitution and regained full protease activity relative to untreated controls upon neutralization (Figure 1B). Moreover, treated GlpG was indistinguishable from untreated GlpG in a sensitive and quantitative structural stability assay (Baker and Urban, 2012), arguing that the pH switch did not alter enzyme structure (Figure 1C). In fact, crystallization of GlpG at neutral and low pH revealed that its overall architecture was unperturbed (Cα rmsd of ~0.32 Å), yet at low pH, the serine side chain was incompetent for catalysis because it had turned away from the histidine (Figure 1D; Table S1 available online), which is consistent with histidine protonation.

Quantitative Analysis of Intramembrane Proteolysis in Real Time

With robust enzyme preparations and this reconstitution method established, we next focused on developing a substrate that would permit monitoring intramembrane proteolysis in real time. Unexpectedly, we discovered that a fluorescein isothiocyanate (FITC) fluorophore attached to the natural amino terminus of a *Providencia stuartii* TatA construct, the only known bacterial rhomboid substrate (Stevenson et al., 2007), was

robustly quenched when reconstituted into proteoliposomes composed of *E. coli* lipids (Figures 2A, 2B, and S1A). In the presence of GlpG, however, a fluorogenic signal was generated at a rate (Figure 2C) that was perfectly coincident with the appearance of the cleaved product as assessed by tricine gel analysis (Figure 2D). Mass spectrometric analysis confirmed that TatA was being cut only at the natural rhomboid cleavage site between alanines 8 and 9 (Stevenson et al., 2007) (Figure 2E). Importantly, both fluorescence and the cleaved product were absent when we mutated either the substrate at the alanine preceding the cleavage site or the GlpG catalytic residues (Figures 2C and 2D). JLK6, an isocoumarin-based rhomboid inhibitor (Vinothkumar et al., 2010), blocked generation of the fluorescence signal and cleavage product (Figures 2C and 2D). Finally, the FITC moiety neither reduced proteolysis (Figure 2D) nor affected the helicity of TatA in membranes as measured by circular dichroism (Figure S1B). Therefore, FITC-TatA cleavage exhibits all the known hallmarks of rhomboid intramembrane proteolysis and permits its monitoring within the membrane in real time.

Steady-State Kinetic Analysis of Proteolysis within the Membrane

To establish controlled conditions for a Michaelis-Menten kinetic system, we lowered GlpG levels to 4 pmol while varying substrate from 20 to 1,600 pmol and coreconstituted both into 200 nm proteoliposomes comprised of *E. coli* lipids to preserve its physiological environment as much as possible (Figure S2A). Under these low enzyme conditions, <5% of the substrate was converted to product in 30 min (Figure 2D), thus satisfying Michaelis-Menten requirements of constant substrate concentrations. Progress curves remained linear for ~60 min before the reactions expectedly slowed due to substrate depletion and product accumulation. Extended incubation times allowed FITC-TatA turnover (Figure S2B), arguing that >85% of the substrate is available to the protease. Finally, FITC-TatA reconstituted in both orientations in approximately equal proportions, as quantified by reacting a single engineered cysteine with a membrane-impermeable dye (Figure 3A). As such, the effective concentration of FITC-TatA per orientation is half of the total amount reconstituted.

Plotting the substrate concentration versus reaction velocity (measured over the first 15 min) produced a rectangular hyperbola that could be fit exceptionally well ($R^2 = 0.99$) with a Michaelis-Menten equation (Figure 3A). Remarkably, the resulting data revealed an extraordinarily high K_M of 0.14 ± 0.02 mole percent (mol%) relative to phospholipid (~1 substrate transmembrane segment per 350 monolayer phospholipids). We verified this measurement independently by tricine gel analysis (Figure S2C). However, because the K_M is more complex than physical affinity alone, we developed a binding assay to measure the K_d between rhomboid and substrate within the membrane directly. We installed a tetramethylrhodamine (TMR) FRET acceptor group onto an extracellular GlpG loop at a site that we previously found does not perturb protein structure (Baker and Urban, 2012). Coreconstituting different amounts of FITC-TatA resulted in an increasing FRET signal from a catalytically inactive mutant of TMR-GlpG that became saturated, revealing an apparent K_d of 0.08 ± 0.026 mol% (Figure 3B), which agrees well with the low affinity revealed by kinetic analysis.

To derive the catalytic turnover rate, k_{cat}, from the measured V_{max}, we quantified the fraction of active protease in our preparations by incubating with JLK6, which is a "suicide inhibitor" that covalently labels only active GlpG (Vinothkumar et al., 2010). Mass spectrometry revealed that ~100% of GlpG in our preparations is catalytically active (Figure 3C), yielding a k_{cat} of 0.0063 ± 0.00021 cuts per second (s^{-1}), or >2.5 min required for a single cleavage event within the membrane when the enzyme is saturated with substrate.

Evaluation of Intramembrane Protease Kinetics in Living Cells

The kinetic parameters governing proteolysis within the membrane were surprisingly inefficient, raising the concern that our reconstitution system may be missing an unknown component or may not accurately reflect physiological conditions. In fact, whereas we have been careful to use lipids purified from growing *E. coli* cells for forming our liposomes, in vitro membrane systems cannot recapitulate potential bilayer asymmetry of lipids, or potential crowding induced by "bystander" proteins, that may be present in natural membranes. We therefore examined the characteristics of rhomboid proteolysis directly in living *E. coli* cells by expressing full-length TatA from an arabinose promoter that allows titration of target protein levels. Using this system, we achieved TatA levels ranging from undetectable to becoming the most abundant protein in the cell membrane (Figure S2D). As expected, increasing TatA resulted in increased intramembrane proteolysis by endogenous GlpG in the natural membranes of living *E. coli* cells (Figure 3D). Cleavage was absent in GlpG knockout cells. Remarkably, even when TatA became the most abundant protein in the cell, GlpG was not yet saturated with substrate, confirming low substrate-binding affinity. Quantifying TatA levels and cleavage yielded a Michaelis-Menten-like curve, with an "apparent in vivo" K_M of 0.19 mol%, which is similar to the 0.14 mol% that we measured in our in vitro reconstitution system.

We also estimated the proteolytic rate in vivo by epitope tagging endogenous GlpG in the *E. coli* chromosome. This was critical because, if we overexpressed GlpG even slightly, we could titrate out any potential stimulatory cofactor or condition. Quantification of endogenous GlpG levels relative to pure protein standards (Figure 3D) yielded an "apparent in vivo" k_{cat} of 0.0069 ± 0.0009 s^{-1}, which again was indistinguishable from the 0.0063 ± 0.00021 s^{-1} that we measured in our reconstitution system. As such, GlpG exhibits low affinity for substrate and slow catalytic rate even in living cells, validating that our reconstitution system faithfully recapitulates physiological conditions for GlpG proteolysis.

The Membrane Environment Slows Rhomboid Proteolysis

Having discovered that the kinetics of proteolysis within the membrane is inefficient, we sought to test whether this reflects limitations imposed by the membrane environment. We examined proteolysis in detergent micelles that support

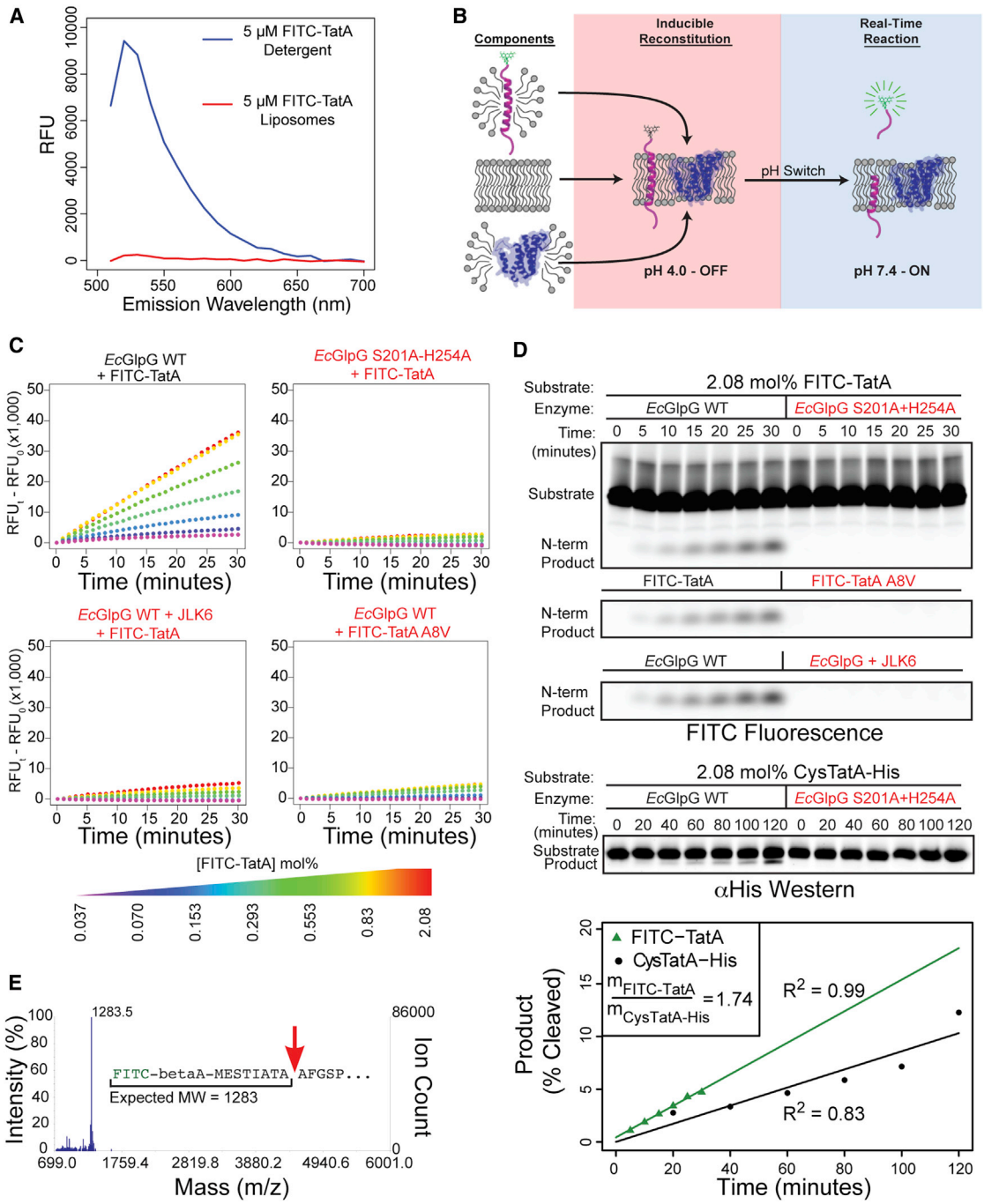

Figure 2. Quantifying Proteolysis within the Membrane in Real Time

(A) FITC-TatA fluorescence is quenched in proteoliposomes (red), but not in detergent micelles (blue). Shown is an emission scan. See Figure S1 for absorption/excitation and circular dichroism scans.

(B) Assay schematic is shown. Transmembrane FITC-TatA and HA-*Ec*GlpG in detergent were coreconstituted into proteoliposomes at pH 4 (red shading), collected by ultracentrifugation, and proteolysis was initiated by neutralization (blue shading). Proteoliposomes quench fluorescence, which is relieved by cleavage-mediated release.

(C) Real-time progress curves at 37°C (read/min) of *Ec*GlpG reconstituted with indicated FITC-TatA concentrations (mol% relative to phospholipids). Mutating *Ec*GlpG or TatA, or pretreating with JLK6, abrogated signal to background.

(D) Fluorescence scan of gel analysis confirmed linear product accumulation (top $R^2 = 0.997$), and sensitivity to mutation/inhibition. Also see Figure S2B for gel analysis of extended incubations. Lower gel and graph indicate that the TatA construct lacking the FITC label was not cleaved more efficiently. N-term, N-terminal.

(E) MALDI-TOF analysis of the N-terminal FITC-TatA cleavage product is shown (red arrow indicates cleavage site).

See also Figure S1.

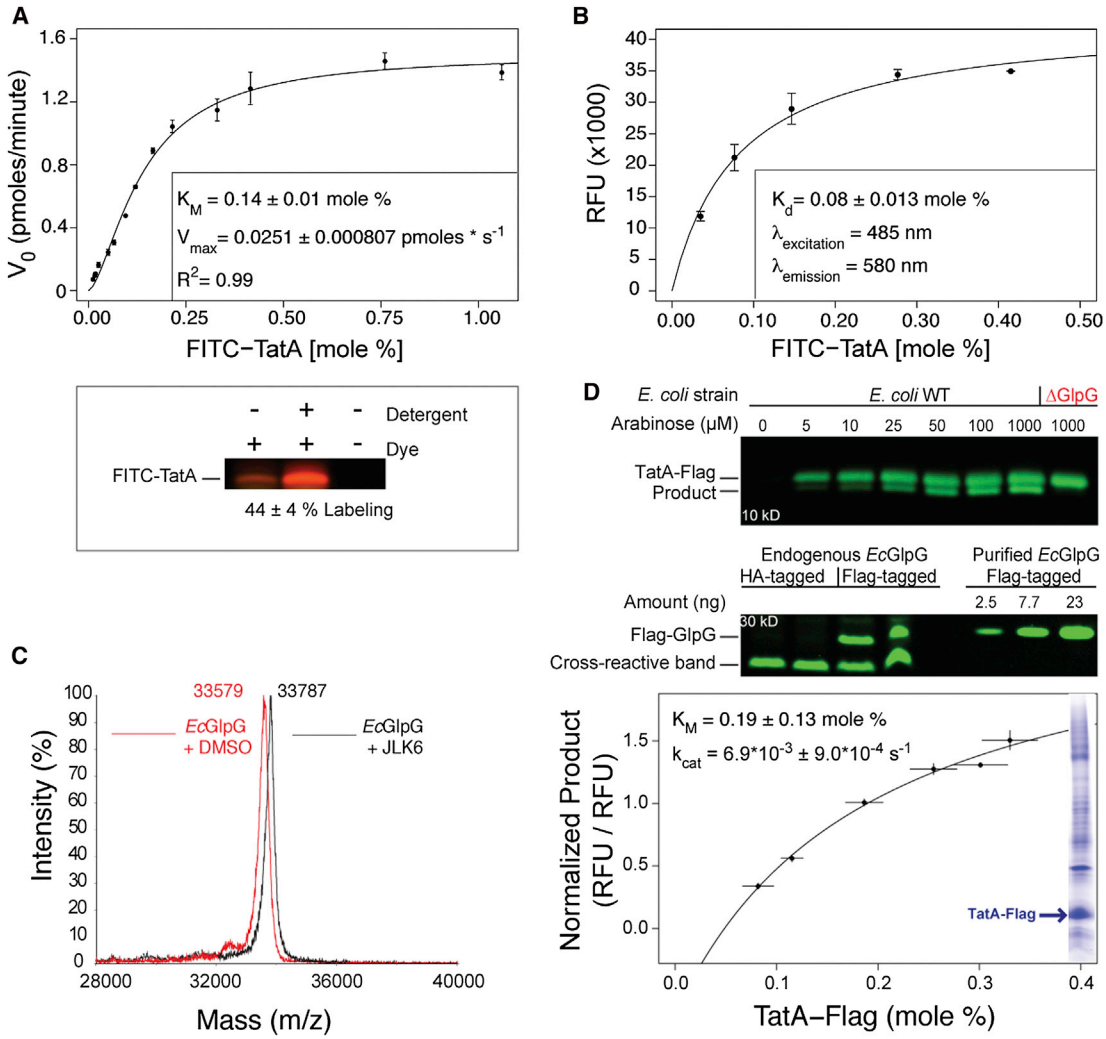

Figure 3. Intramembrane Proteolysis Kinetics and Equilibrium Binding Parameters inside the Membrane

(A) Real-time kinetics of FITC-TatA cleavage by *Ec*GlpG in proteoliposomes was fit with a Michaelis-Menten model (mean ± SEM, n = 2, inset shows fit ± SD). Gel image (below) quantifying FITC-TatA-Cys labeling by a membrane-impermeable thiol-reactive dye, revealing half of TatA reconstituted with its amino terminus facing the liposome interior. The reconstitution efficiency was consistent between experiments (see Figure S2A). Reactions were also analyzed on 16% tricine gels, and products were quantified and plotted (see Figures S2B and S2C).

(B) Binding of FITC-TatA to catalytically inactive TMR-GlpG (C104A+W196TMR+H254A) in proteoliposomes is shown. Plotted is background-subtracted FRET intensity versus mole fraction of FITC-TatA (relative to phospholipids). K_d was derived from the curve fit.

(C) Mass spectra of *Ec*GlpG incubated with the activity-based inhibitor JLK6 produced a complete mass shift, revealing that all purified *Ec*GlpG is active.

(D) TatA-Flag cleavage in *E. coli* cells by endogenous GlpG is shown. TatA expression levels were titrated with arabinose, and cleavage was assessed by anti-Flag western blot (upper gel). Deleting genomic GlpG (ΔGlpG) resulted in no cleavage. Levels of endogenous GlpG (Flag tagged by knockin) were quantified in duplicate relative to known Flag-GlpG pure protein standards by anti-Flag western blot (lower gel). Cross-reactive bands served as loading controls. Graph indicates that half-maximal cleavage by endogenous GlpG occurred when TatA reached 0.19 mol% (relative to phospholipids). Also shown (inset) is a Coomassie blue-stained SDS-PAGE gel revealing that TatA became 20% of the *E. coli* membrane proteome when induced with 1 mM arabinose (also see Figure S2D). See also Figure S2.

high rhomboid activity and found a strikingly high K_M of at least 135 ± 16.6 μM, with V_{max} approached at >300 μM substrate (Figure 4A). The V_{max} we measured is ~10 times faster than previously measured for rhomboid proteases in detergent (Lazareno-Saez et al., 2013), suggesting that prior studies did not saturate enzyme with substrate but instead suffered plateauing for another reason, such as substrate aggregation at higher concentrations and extended incubation times of 2 hr.

A way to distinguish between indirect effects and true binding is to measure the K_d directly between rhomboid and substrate, which has never been achieved for any intramembrane protease. Commonly used gel filtration and coprecipitation approaches indicated a low affinity of >800 μM (Figures 4B and 4C). Because these approaches separate complex from monomers, they promote dissociation and thus can overestimate K_d. We therefore performed equilibrium gel filtration

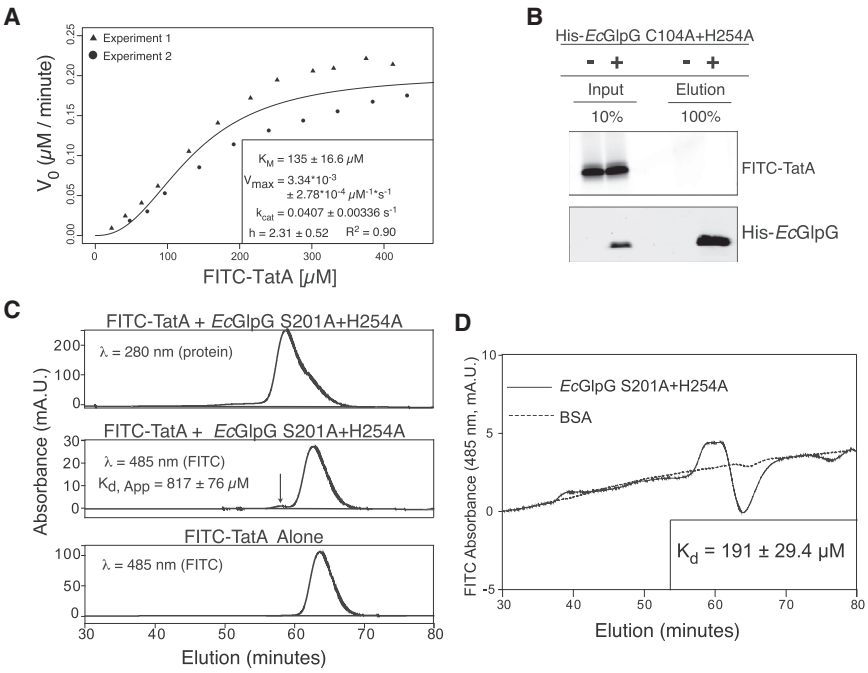

Figure 4. Intramembrane Proteolysis Kinetics and Equilibrium Binding Analyzed in Three Dimensions

(A) Michaelis-Menten plot shows FITC-TatA cleavage by HA-*Ec*GlpG in detergent micelles (inset shows fit ± SD). Variation increased at >100 μM due to variable solubility of the transmembrane substrate.

(B) Analysis of FITC-TatA coprecipitation with the inactive mutant His-*Ec*GlpG C104A+H254A is shown. Quantification revealed that <0.1% of FITC-TatA eluted with His-*Ec*GlpG, which, under nonequilibrium conditions, corresponds to an apparent K_d of ≥1 mM.

(C) HPLC gel filtration analysis of FITC-TatA mixed with HA-*Ec*GlpG S201A+H254A reveals a small complex peak (arrow), which is absent in the elution profile of FITC-TatA alone. The single A_{280} (protein absorption) peak is an overlap of HA-*Ec*GlpG (eluting first) and FITC-TatA (right shoulder). mA.U., milliabsorbance units.

(D) HPLC equilibrium gel filtration analysis of FITC-TatA/*Ec*GlpG (inactive S201A+H254A mutant) complex versus FITC-TatA/BSA control run on a column equilibrated with 9.5 μM FITC-TatA. The A_{485} (FITC absorption) peak corresponds to the GlpG-TatA complex, whereas the trough results from FITC-TatA depletion from the mobile phase due to GlpG binding (peak/trough absence with BSA indicates no binding).

(Hummel and Dreyer, 1962) by pre-equilibrating the entire column with substrate. Under these equilibrium conditions, the K_d between rhomboid and substrate was 191 ± 29.4 μM (Figure 4D), which is in excellent agreement with our measured K_M. These values indeed suggest that rhomboid does not display even modest natural affinity for substrates in any environment.

Interestingly, however, k_{cat} was ~6.5-fold faster in detergent than in proteoliposomes (Figure 4A), revealing that the membrane environment slows proteolysis. It is generally accepted that hydrolysis within the membrane, where water is scarce, is rate limiting for proteolysis. To test this directly, we performed a kinetic solvent isotope effect analysis by substituting deuterium oxide for water. A decrease in rate in deuterium oxide is commonly used to identify a rate-limiting hydrolysis step in a reaction (Fersht, 1999). Surprisingly, hydrolysis itself was not rate limiting in membranes because the ratio of the water:deuterium oxide proteolysis rates for GlpG was only a modest 1.26 ± 0.32 (Figure 5A) instead of the expected ≥2 for serine proteases (Elrod et al., 1980; Zhang and Kovach, 2006). In contrast, such mild effects are often caused by deuterium exchange with protein groups, and indeed, we observed a gradual effect on proteolysis when we titrated deuterium oxide in the presence of water (Figure 5B). This is diagnostic of an equilibrium effect on protein, rather than a direct effect on hydrolytic rate (Fersht, 1999).

Conversely, we found that substrate gating plays a major role in determining reaction rate in the membrane (Figure 5C). Analysis of gate-open relative to wild-type GlpG revealed a >3-fold increase in k_{cat} without any change in K_M (Figure 5C) or cleavage site (Figure S3), arguing that gate opening is the rate-limiting step for proteolysis within the membrane. Although recent structural studies with covalent inhibitors have suggested that gating residues contribute to substrate binding (Xue and Ha, 2012), mutants in these residues do not change K_M. The membrane environment thus slows proteolytic rate, in part, by restraining protease gate opening, but K_M appears to be inherently inefficient in all settings.

Kinetic Analysis of Diverse Rhomboid Proteases Reveals a Common Mechanism

To our knowledge, it is unprecedented for the K_M of a specific protease to play little or no role in driving proteolysis under physiological conditions (Perona and Craik, 1997; Timmer et al., 2009). To evaluate this possibility further, we characterized the effect of both protease and substrate variants.

Although *E. coli* GlpG is currently the best-characterized intramembrane protease, rhomboid proteases vary greatly in sequence (Lemberg and Freeman, 2007) and specific activity (Urban and Wolfe, 2005). We therefore measured the kinetic parameters for a panel of nine diverse rhomboid proteases that share <3% sequence identity (Figures 6A, 6B, and S3). Remarkably, despite varying ~10,000-fold in specific activity, all nine rhomboid proteases displayed indistinguishable K_M values (Figure 6C). In fact, even AarA, the natural protease that coevolved with TatA (Stevenson et al., 2007), had, if anything, a slightly higher (less efficient) K_M for TatA than GlpG (Figures 6A–6D). Conversely, all differences in protease activity across this diverse panel of enzymes, when analyzed under identical conditions, were reflected in k_{cat} changes alone, which ranged ~10,000-fold (Figures 6C and 6D).

Comparing a diverse set of rhomboid proteases to *E. coli* GlpG required maintaining equivalent conditions. As a result, a few

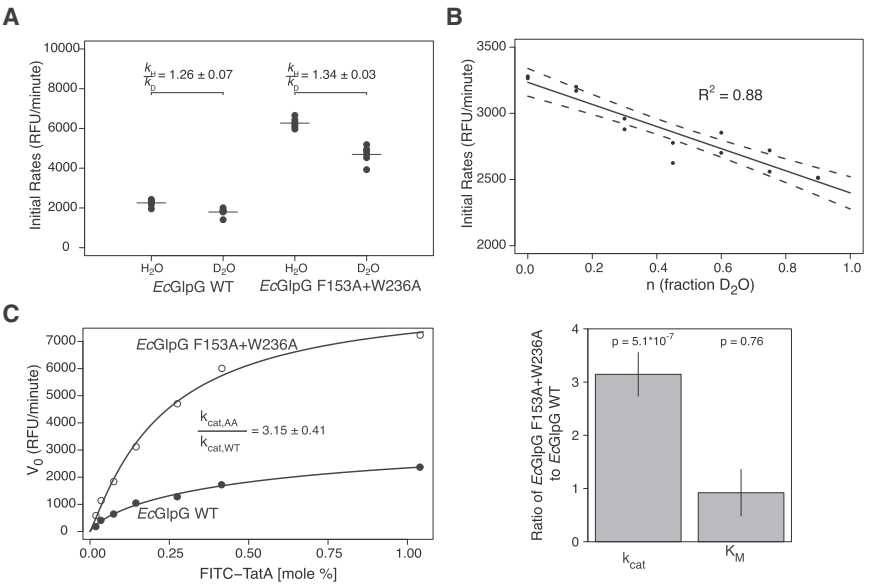

Figure 5. Rate-Limiting Step Analysis for Rhomboid Proteolysis inside the Membrane

(A) Rate analysis of FITC-TatA cleavage by *Ec*GlpG in proteoliposomes in the presence of H_2O versus D_2O is shown. The weak (<2) effect of D_2O (expressed as a rates ratio) indicates that hydrolysis is not rate limiting.

(B) Titration analysis of FITC-TatA cleavage rate by *Ec*GlpG in proteoliposomes in the presence of different proportions of D_2O is presented. The linear effect indicates that the slowing is due to perturbation of an equilibrium (exchange with protein groups), not a rate (hydrolysis step), effect.

(C) Parallel real-time kinetic analysis of FITC-TatA cleavage by wild-type (filled circles) versus gate-open (F153A+W236A, open circles) *Ec*GlpG in proteoliposomes was fit (left panel) with a Michaelis-Menten model (mean ± SEM, n = 2; inset shows fit ± SD). Bar graph presents comparison (right panel) of the gate-open mutant effect on k_{cat} (~3-fold faster) and K_M (no change). See Figure S3 for cleavage site generated by gate-open GlpG.

rhomboid proteases were assayed under conditions that were physiological for *E. coli* GlpG but different from what they would experience normally. Because these enzymes generally appeared less active than GlpG, we re-evaluated their activity under more physiological conditions. *Aquifex aeolicus* is an extreme thermophilic organism with a growth optimum of 85°C (Deckert et al., 1998). Analysis of *Aquifex aeolicus* rhomboid (AqROM) at 85°C revealed a 250-fold increase in protease activity, all of which was reflected in a higher k_{cat} with no corresponding decrease in K_M (Figures 6B–6D). Similarly, although bacteria do not make phosphatidylcholine, the membranes of *Pseudomonas aeruginosa* accrue 4% phosphatidylcholine (and potentially other lipid species) because it assimilates choline during infection of its host (Wilderman et al., 2002). Analysis of PaROM revealed a >5-fold stimulation of its protease activity, but not that of other rhomboid proteases, by phosphatidylcholine, that again was accounted for by an increase in k_{cat} (Figures 6C, 6D, and S4). Collectively, these observations strongly support our discovery that intramembrane proteolysis is fundamentally governed by k_{cat}, with little or no contribution from substrate-binding affinity.

Kinetic Analysis of Substrate Mutants Reveals No Binding Affinity Motif

We also examined defined substrate mutants that have been under investigation for over a decade, but the lack of a kinetic system precluded rigorous mechanistic interpretation for how they affect proteolysis (reviewed in Urban, 2010). TatA itself has been subjected to extensive mutational analysis with >150 mutants, the outcome being interpreted as identification of a "recognition motif" for sequence-specific binding comprised of large residues four residues preceding, and two residues following, the cleavage site (Strisovsky et al., 2009). We therefore examined a double mutant with disallowed alanines at these positions and indeed found that proteolysis was decreased >100-fold (Figure 7A). However, contrary to expectation for a sequence-binding motif, the mutant substrate actually decreased K_M ($p = 0.00073$), implying 4-fold improved binding (Figure 7B)! This result was also reassuring because it demonstrated that our assay was capable of measuring high affinity. The decrease in the processing of the TatA double mutant was instead reflected in a >100-fold decrease in k_{cat}, which itself may account for the lower K_M (Figures 7B and 7C). Overall, these findings are completely consistent with prior observations, including mutagenesis data, but reveal that mutating apparent sequence motifs in substrates lowers proteolysis not by abrogating binding affinity (K_M not increased) but by altering optimal exposure of the peptide bond for efficient hydrolysis (lowered k_{cat}).

Like all studied rhomboid substrates, TatA contains a region deeper within its transmembrane segment composed of helix-destabilizing residues that facilitate substrate unwinding prior to proteolysis (Moin and Urban, 2012; Strisovsky et al., 2009). A mutant in these residues decreased TatA cleavage but again reduced k_{cat} without raising K_M (Figures 7B and 7C). Finally, the *Drosophila* signaling molecule Spitz, which is a less-efficient substrate than TatA, also displayed lower k_{cat} without any significant change in K_M (Figures 7B and 7C). Together, these defined substrate variants further indicate that intramembrane proteolysis is a kinetically controlled reaction that is not driven by affinity between protease and substrate.

DISCUSSION

In summary, we have developed an inducible reconstitution system for the analysis of intramembrane proteolysis in real time. This allowed us to measure the kinetic parameters of proteolysis occurring directly inside the membrane. Although the rhomboid domain is defined as a transmembrane segment binding moiety (Adrain and Freeman, 2012), all data with nine

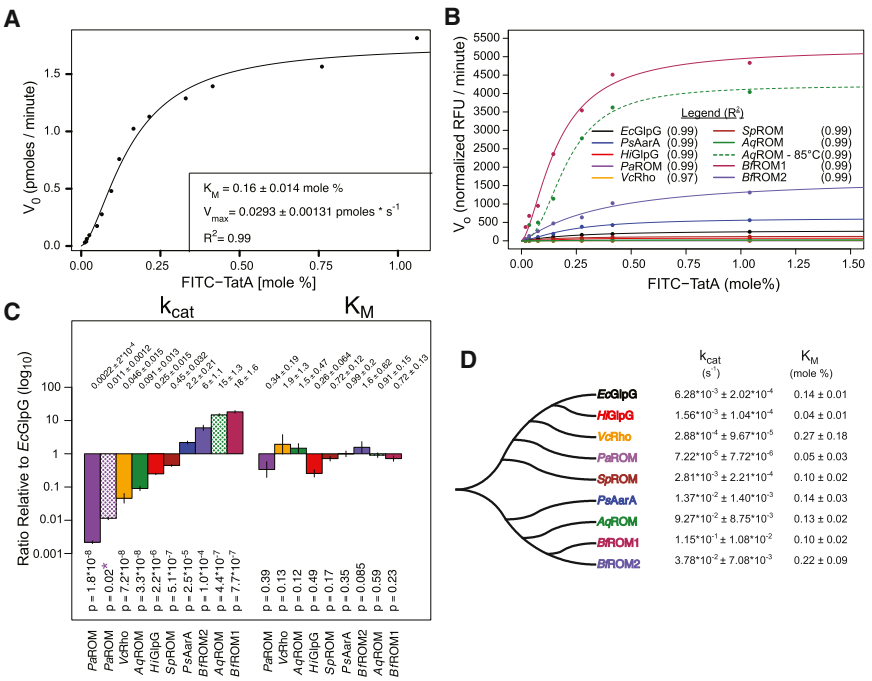

Figure 6. Kinetics of Membrane-Immersed Proteolysis by Nine Diverse Rhomboid Proteases

(A) Michaelis-Menten model fit (inset shows fit ± SD) to real-time reaction velocity of FITC-TatA processing by HA-*Providencia stuartii* AarA (HA-*Ps*AarA) in proteoliposomes.

(B) Michaelis-Menten graphs illustrate direct pairwise comparisons of eight diverse rhomboid proteases to HA-*Ec*GlpG (*Hi*GlpG, *Haemophilus influenzae* GlpG; *Pa*ROM, *Pseudomonas aeruginosa* ROM; *Vc*Rho, *Vibro cholerae* Rho; *Sp*ROM, *Streptococcus pneumoniae* ROM; *Aq*ROM; and *Bf*ROM1/*Bf*ROM2, *Bacteroides fragilis*). See Figure S4A for protein sequence alignment and accession numbers.

(C) Comparison of kinetic parameters derived from Michaelis-Menten model fits is presented (above shows the ratios ± SD, and below indicates the p values of pairwise model fitting with Bonferroni correction of k_{cat} values). Patterned bars indicate when *Aq*ROM was analyzed at 85°C, and *Pa*ROM was analyzed in liposomes composed of DMPC (asterisk denotes comparison to *Pa*ROM in *E. coli* liposomes). Also see Figure S4B for *Pa*ROM (slowest enzyme analyzed) labeling.

(D) A phylogenetic tree of analyzed rhomboid proteases and their best Michaelis-Menten parameters (fitted values ± SD) are shown. Data are color coded throughout the figure.

See also Figure S4.

different rhomboid proteases and five substrate variants reveal that protease and substrate have little, if any, meaningful affinity for each other within the membrane. This conclusion is independently supported by direct measurements of K_d in the membrane using a FRET-based assay, and in detergent micelles by a variety of approaches including equilibrium gel filtration. Although our reconstitution system necessarily uses pure proteins to allow precise measurements, estimating "apparent" kinetic parameters in living *E. coli* cells indicates that it faithfully recapitulates in vivo rhomboid properties. Lack of need for other cofactors is also consistent with divergent rhomboid enzymes rescuing mutant defects in radically different organisms (Gallio et al., 2002) and no additional components being uncovered in many saturation screens performed over the course of decades in both eukaryotes and prokaryotes (Casci and Freeman, 1999; Rather et al., 1999).

The central implication of the kinetic parameters is that proteolysis within the membrane is not driven by substrate affinity under physiological conditions. It is important to note that it is not the absolute K_M value itself that leads to this conclusion: whereas some proteases like chymotrypsin also display high K_M values (Wysocka et al., 2008), these digestive proteases encounter food protein at extraordinarily high and thus matched concentrations. Instead, although there is little precedent for interpreting binding affinities within two dimensions, a K_M of ~0.14 mol% is extraordinarily high because the inner membrane of *E. coli* contains only 1.25–1.67 mol% (~50% by weight) of total protein (Schnaitman, 1970a, 1970b). Indeed, experimentally, we found that substrate has to become nearly the most abundant protein in the *E. coli* membrane to be near K_M and constitute all protein in a membrane to even approach V_{max}. Compared to other signaling proteases, rhomboid proteases are thus at least 100-fold less efficient: the catalytic efficiency (k_{cat}/K_M) of *E. coli* GlpG, the best-understood intramembrane protease, is only ~47 $M^{-1}s^{-1}$ (0.0063 s^{-1}/135 μM) relative to >10,000 $M^{-1}s^{-1}$ for caspases (Stennicke et al., 2000; Timmer et al., 2009).

Instead, these properties force us to consider that membrane-immersed proteolysis may be organized differently from other forms of proteolysis. All changes we observed involve k_{cat}, revealing that intramembrane proteolysis is fundamentally a kinetically controlled reaction, rather than relying on differences in protein affinity (i.e., not thermodynamically controlled). Interestingly, these enzymatic properties are unlike those of other studied proteases or membrane proteins but strikingly parallel those of one subset of DNA repair enzymes.

DNA glycosylases remove damaged bases from DNA using an intriguing mechanism that involves two different enzyme sites (Figure 7D). Nucleotides flipped out of a DNA double helix first interact with an "interrogation site" on the DNA glycosylase (Friedman and Stivers, 2010). Importantly, a damaged base is not bound with high affinity per se; instead, it is able to spend more time in the dynamic, extrahelical state and thus stay longer in the interrogation complex. This longer residence allows the base to translocate to a second, deeper site—the excision site—where the glycosidic linkage is clipped to excise the base from DNA. The discriminatory mechanism is therefore rate governed, with a minor contribution from binding affinity to the damaged base itself. The second key property of these DNA glycosylases is a slow k_{cat} because it ensures that catalysis is

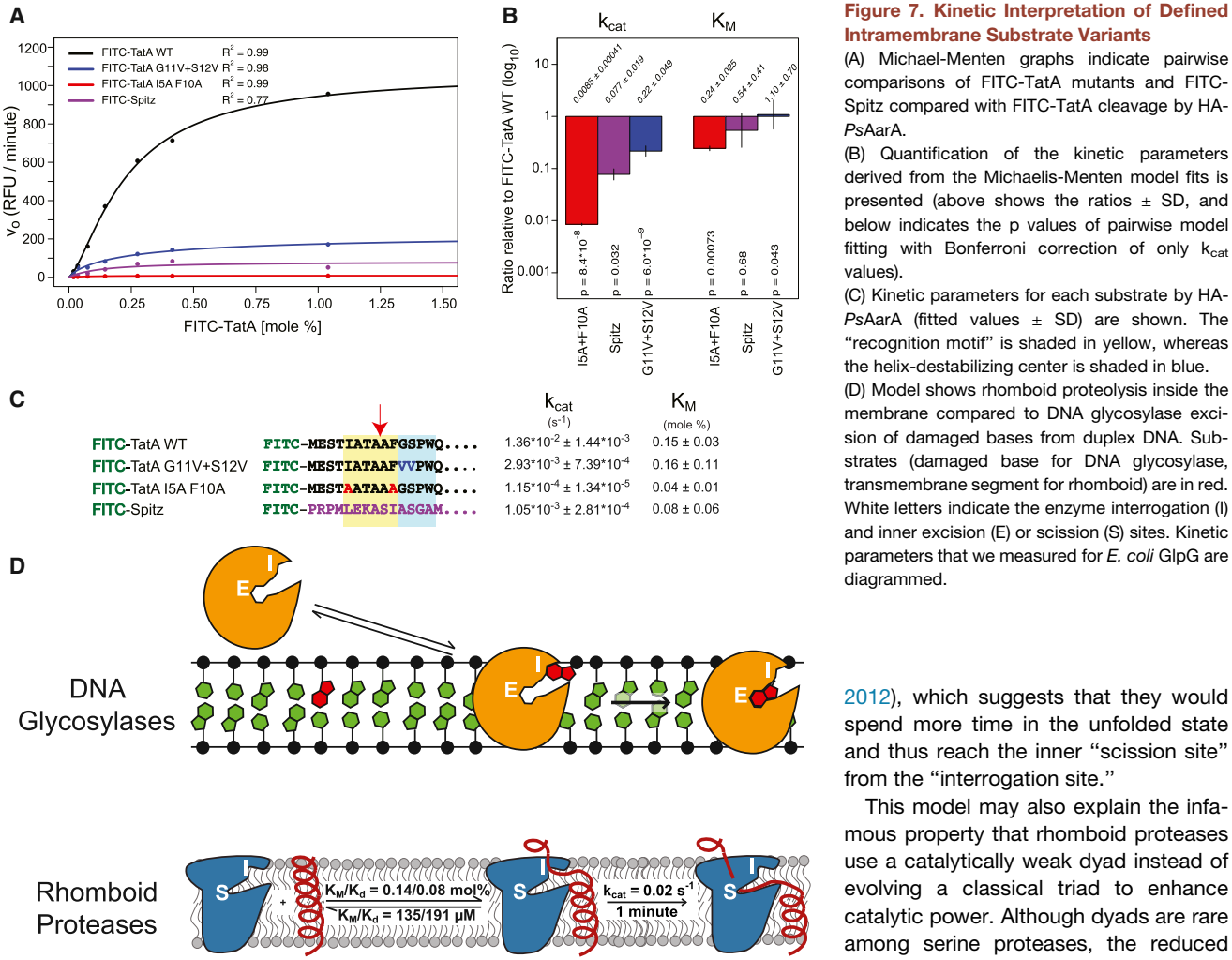

Figure 7. Kinetic Interpretation of Defined Intramembrane Substrate Variants

(A) Michael-Menten graphs indicate pairwise comparisons of FITC-TatA mutants and FITC-Spitz compared with FITC-TatA cleavage by HA-*Ps*AarA.

(B) Quantification of the kinetic parameters derived from the Michaelis-Menten model fits is presented (above shows the ratios ± SD, and below indicates the p values of pairwise model fitting with Bonferroni correction of only k_{cat} values).

(C) Kinetic parameters for each substrate by HA-*Ps*AarA (fitted values ± SD) are shown. The "recognition motif" is shaded in yellow, whereas the helix-destabilizing center is shaded in blue.

(D) Model shows rhomboid proteolysis inside the membrane compared to DNA glycosylase excision of damaged bases from duplex DNA. Substrates (damaged base for DNA glycosylase, transmembrane segment for rhomboid) are in red. White letters indicate the enzyme interrogation (I) and inner excision (E) or scission (S) sites. Kinetic parameters that we measured for *E. coli* GlpG are diagrammed.

slower than the residence time of natural bases, kinetically protecting them from hydrolysis (Friedman and Stivers, 2010).

These striking parallels suggest that low substrate affinity and slow rate of rhomboid proteolysis are not defects but, rather, features of this enzyme system. Moreover, they offer a mechanistic framework for interpreting how membrane-immersed proteolysis is organized (Figure 7D). First, the lack of affinity for substrates and reliance on rates suggest that rhomboid proteases may also use an analogous "interrogation" site to discriminate substrate from nonsubstrate kinetically. Although the gate has been viewed simply as a point of substrate entry, the crevice created by gate opening, which is stable in the membrane (Urban and Baker, 2008; Zhou et al., 2012), may actually be an "interrogation" site (Figure 7D). Like with DNA glycosylases, this site is physically separated from the deeper active site, which would force transmembrane helices to reside in the unwound state to reach the catalytic residues for proteolysis to ensue (Figure 7D), instead of returning laterally to the membrane. Our recent spectroscopy analysis of substrates revealed that they form inherently less-stable helices than nonsubstrates (Moin and Urban, 2012), which suggests that they would spend more time in the unfolded state and thus reach the inner "scission site" from the "interrogation site."

This model may also explain the infamous property that rhomboid proteases use a catalytically weak dyad instead of evolving a classical triad to enhance catalytic power. Although dyads are rare among serine proteases, the reduced catalytic rate would help protect nonsubstrates kinetically from cleavage by ensuring sufficient time for them to escape back into the membrane before cleavage could occur. In fact, the slow k_{cat} of 0.02 s^{-1} that we measured for gate-open GlpG is much like the k_{cat} of 0.03 s^{-1} exhibited by human DNA glycosylase OGG1 (Kuznetsov et al., 2007).

It is thus tempting to speculate that the primordial function of rhomboid proteases was to patrol the membrane looking for unfolded membrane proteins to cleave as a repair mechanism analogous to how DNA glycosylases patrol the genome for damaged bases. Nevertheless, because comparing intramembrane proteases to DNA repair enzymes is entirely new, it requires focused testing to determine to what degree rhomboid function is like that of DNA glycosylases and where it deviates. Our discovery also has practical implications for inhibitor design; because substrate affinity is low, commonly used strategies that rely on substrate characteristics to target inhibitor warheads to proteases (Drag and Salvesen, 2010) are unlikely to produce potent compounds against rhomboid. Likewise, caution should be exercised when interpreting covalent inhibitor-bound GlpG structures in what they can teach us about natural substrate binding (Vinothkumar et al., 2010; Xue et al., 2012). On an

optimistic note, a robust kinetic system will allow evaluating inhibitors based on precise K_i values and directly within membranes, instead of relying on IC_{50} concentrations that are condition dependent.

We focused our analyses on rhomboid proteases, but it should be noted that such quantitative real-time analyses have yet to be realized with other intramembrane proteases. In fact, a major achievement is the recent application of kinetic analysis to γ-secretase (Chávez-Gutiérrez et al., 2012), albeit in detergent extracts and with endpoint assays. In this light, a particularly exciting feature of our system is its potential to be applied broadly: all protease catalysis is pH sensitive, and similar placement of a FITC label should also afford natural quenching of other substrates upon membrane reconstitution. Alternatively, γ-secretase and site-2 proteases could be switched on after reconstitution by washing out reversible inhibitors or supplying zinc ions, respectively. It is possible that some intramembrane proteases like γ-secretase could exhibit different kinetics because they evolved extramembranous domains for substrate binding (Fleig et al., 2012; Li et al., 2009; Shah et al., 2005). However, because these are later adaptations, low intramembrane affinity may be a primordial and common property of intramembrane proteolysis. Whether weak binding at transmembrane sites is important for catalysis inside the membrane, or a deliberate specialization by this class of enzymes, remains to be determined.

EXPERIMENTAL PROCEDURES

Protein Purification

Each HA-rhomboid protein was expressed and purified as described previously (Baker and Urban, 2012; Urban and Wolfe, 2005). Briefly, glutathione S-transferase (GST) fusion proteins were expressed in *E. coli* C43 (DE3) cells, purified with glutathione Sepharose (GE Healthcare), and eluted by on-column PreScission cleavage to remove the GST tag. Purity of each enzyme was determined by SDS-PAGE stained with Coomassie colloidal blue and quantified on an Odyssey imager (LI-COR Biosciences). To avoid erroneous quantitation from inherent differences in Coomassie staining of different rhomboid proteins, all enzymes were standardized by anti-HA analysis in parallel as quantified on an Odyssey imager.

C-terminal Flag-tagged recombinant substrate APP-Spi7-Flag was expressed and purified from *E. coli* as described (Baker and Urban, 2012; Baker et al., 2007). FITC-TatA (residues 1–33 of 97) and Spitz (residues 135–168 of 186) substrates containing the entire transmembrane segment were synthesized by Fmoc solid-state chemistry, with FITC conjugated to the N terminus through a β-alanine linkage, and an amidated C terminus, and resuspended in 50 mM Tris (pH 7.4), 150 mM NaCl, 1 mM DTT, and 0.2% (w/v) Sarkosyl. The actual final concentration of each substrate preparation was quantified using FITC fluorescence relative to FITC standards using a Synergy H4 Hybrid plate reader (BioTek).

E. coli Liposome Preparation

A total of 100 mg of *E. coli* polar lipid extract in chloroform (Avanti Polar Lipids) was slowly dried into a thin lipid film in a rotary evaporator and dried under high vacuum overnight on a custom-made glass manifold (Kontes Glass). The film was then resuspended thoroughly in 10 ml of 10 mM HEPES (pH 7), 10 mM NaCl, and 1 mM DTT, briefly sonicated in a temperature-controlled sonifier (Branson), and extruded through 200 nm pore filters to form liposomes of defined size.

Inducible Reconstitution and Real-Time Proteolysis Assay

A total of 30 μg of *E. coli* liposomes was mixed with 50 mM NaAcetate (pH 4.0), 150 mM NaCl, 0.05–500 pmol of rhomboid enzyme, and 20–1,600 pmol of FITC substrate. This coreconstitution mix was diluted 20-fold with 12.5 mM NaAcetate (pH 4.0), 37.5 mM NaCl to reduce detergent below its critical micelle concentration and promote reconstitution. Proteoliposomes were collected by ultracentrifugation at 600,000 × *g* for 20 min in an Optima MAX-XP ultracentrifuge (Beckman). The supernatant was removed by aspiration, the pellet was resuspended in 50 mM Tris (pH 7.4), 150 mM NaCl, and 1 mM DTT to initiate proteolysis (in the presence of D_2O for isotope experiments), rapidly transferred into a prewarmed black 384-well microtiter plate, covered with film to prevent evaporation, and incubated at 37°C in a Synergy H4 Hybrid plate reader (BioTek). Fluorescence was monitored every minute using monochromators set to wavelengths of 485 ± 20 nm (excitation) and 528 ± 20 nm (emission). Alternatively, time points were quenched with equal volumes of 2× Tricine SDS-sample buffer, resolved on 16% Tricine gels (Life Technologies), and imaged with a blue laser and fluorescein emission filters on a Typhoon Imager (GE Healthcare). APP-Spi7-Flag and HA-*Ec*GlpG were coreconstituted as above, resolved by SDS-PAGE, detected by two-color anti-Flag and anti-HA western analysis, and imaged with an Odyssey infrared scanner (LI-COR Biosciences).

In Vivo TatA-Flag Titration

Expression of TatA-Flag (full-length protein with a C-terminal Flag tag) in log-phase *E. coli* K12 BW25113 cells was titrated using arabinose-mediated induction from a pBAD plasmid. Induced cultures were grown at 37°C in a shaking incubator for 2 hr. Cleavage by endogenous GlpG was quantified by resolving cell lysates on a 16% Tricine SDS-PAGE gel, followed by anti-Flag western analysis and imaging with an Odyssey infrared scanner. To quantify expression levels of TatA-Flag, cells were lysed in a French pressure cell (two passes at 16,000 psi), and the lysate was clarified to remove unbroken cells at 9,000 × *g* for 8 min in a JLA 8.1000 rotor (Beckman). Membranes were collected by ultracentrifugation at 50,000 rpm for 1 hr in a MLA-55 rotor (Beckman). Peripheral and contaminating soluble proteins were removed with a sodium carbonate wash. Total membrane protein from each titration was separated on a 4%–20% tris-glycine SDS-PAGE gel, stained with a colloidal Coomassie blue dye (LI-COR Biosciences) and quantified with an Odyssey infrared scanner. TatA-Flag expression was converted to the molar ratio of membrane proteins by correcting signals for molecular weight, then converted to mol% of membranes. To estimate k_{cat} in vivo, endogenous Flag-*Ec*GlpG levels in membranes prepared by sucrose gradient ultracentrifugation were quantified by western analysis relative to purified Flag-*Ec*GlpG as a standard.

Fitting and Statistical Analysis

All data were analyzed and graphed using the R language and environment. Initial rates were extracted from real-time curves between 4 and 14 min using the slope (m) in a linear model: $y = mx + b$. Initial rates versus substrate concentration of reconstituted reactions were modeled using the Hill-modified Michaelis-Menten equation: $v_0 = (V_{max} \times [S_0]^h)/(K_m{}^h + [S_0]^h)$. Importantly, we did not observe cooperativity with reconstituted reactions analyzed by SDS-PAGE, indicating that cooperativity is not a true feature of the enzyme reaction. p values in pairwise comparisons were derived from multiple nonlinear regression analysis, and k_{cat} p values were corrected for multiple comparisons using the Bonferroni method (K_M p values were not corrected because none achieved significance). See Extended Experimental Procedures for more information.

ACCESSION NUMBERS

Coordinates and structure factors have been deposited in the Protein Data Bank under the ID code 4NJN.

SUPPLEMENTAL INFORMATION

Supplemental Information includes Extended Experimental Procedures, four figures, and one table and can be found with this article online at http://dx.doi.org/10.1016/j.cell.2013.10.053.

AUTHOR CONTRIBUTIONS

S.U. designed the study. R.P.B. and S.U. developed the inducible coreconstitution system. S.W.D. developed the real-time assay, performed all experiments except those in Figures 1A, 1B, 1D, and S1B, and prepared the figures. S.C. solved the structure of GlpG at neutral and low pH. S.U. wrote the paper, and all authors approved the final manuscript.

ACKNOWLEDGMENTS

This work was supported by NIH grant 2R01AI066025, the Howard Hughes Medical Institute, and the David and Lucile Packard Foundation. Part of this research was conducted using instruments at the Malaria Research Institute Biophysics Core (CD spectrometer), and CHESS (beamline supported by NSF grant DMR-0936384 and NIH grant GM-103485).

Received: March 22, 2013
Revised: August 4, 2013
Accepted: October 28, 2013
Published: December 5, 2013

REFERENCES

Adrain, C., and Freeman, M. (2012). New lives for old: evolution of pseudoenzyme function illustrated by iRhoms. Nat. Rev. Mol. Cell Biol. *13*, 489–498.

Baker, R.P., and Urban, S. (2012). Architectural and thermodynamic principles underlying intramembrane protease function. Nat. Chem. Biol. *8*, 759–768.

Baker, R.P., Young, K., Feng, L., Shi, Y., and Urban, S. (2007). Enzymatic analysis of a rhomboid intramembrane protease implicates transmembrane helix 5 as the lateral substrate gate. Proc. Natl. Acad. Sci. USA *104*, 8257–8262.

Casci, T., and Freeman, M. (1999). Control of EGF receptor signalling: lessons from fruitflies. Cancer Metastasis Rev. *18*, 181–201.

Chávez-Gutiérrez, L., Bammens, L., Benilova, I., Vandersteen, A., Benurwar, M., Borgers, M., Lismont, S., Zhou, L., Van Cleynenbreugel, S., Esselmann, H., et al. (2012). The mechanism of γ-Secretase dysfunction in familial Alzheimer disease. EMBO J. *31*, 2261–2274.

Deckert, G., Warren, P.V., Gaasterland, T., Young, W.G., Lenox, A.L., Graham, D.E., Overbeek, R., Snead, M.A., Keller, M., Aujay, M., et al. (1998). The complete genome of the hyperthermophilic bacterium *Aquifex aeolicus*. Nature *392*, 353–358.

De Strooper, B., and Annaert, W. (2010). Novel research horizons for presenilins and γ-secretases in cell biology and disease. Annu. Rev. Cell Dev. Biol. *26*, 235–260.

Doucet, A., Butler, G.S., Rodríguez, D., Prudova, A., and Overall, C.M. (2008). Metadegradomics: toward in vivo quantitative degradomics of proteolytic post-translational modifications of the cancer proteome. Mol. Cell. Proteomics *7*, 1925–1951.

Drag, M., and Salvesen, G.S. (2010). Emerging principles in protease-based drug discovery. Nat. Rev. Drug Discov. *9*, 690–701.

Elrod, J.P., Hogg, J.L., Quinn, D.M., Venkatasubban, K.S., and Schowen, R.L. (1980). Protonic reorganization and substrate structure in catalysis by serine proteases. J. Am. Chem. Soc. *102*, 3917–3922.

Fersht, A. (1999). Structure and Mechanism in Protein Science: A Guide to Enzyme Catalysis and Protein Folding (New York: W.H. Freeman and Company).

Fleig, L., Bergbold, N., Sahasrabudhe, P., Geiger, B., Kaltak, L., and Lemberg, M.K. (2012). Ubiquitin-dependent intramembrane rhomboid protease promotes ERAD of membrane proteins. Mol. Cell *47*, 558–569.

Fluhrer, R., Steiner, H., and Haass, C. (2009). Intramembrane proteolysis by signal peptide peptidases: a comparative discussion of GXGD-type aspartyl proteases. J. Biol. Chem. *284*, 13975–13979.

Friedman, J.I., and Stivers, J.T. (2010). Detection of damaged DNA bases by DNA glycosylase enzymes. Biochemistry *49*, 4957–4967.

Gallio, M., Sturgill, G., Rather, P., and Kylsten, P. (2002). A conserved mechanism for extracellular signaling in eukaryotes and prokaryotes. Proc. Natl. Acad. Sci. USA *99*, 12208–12213.

Hummel, J.P., and Dreyer, W.J. (1962). Measurement of protein-binding phenomena by gel filtration. Biochim. Biophys. Acta *63*, 530–532.

Huntington, J.A. (2012). Thrombin plasticity. Biochim. Biophys. Acta *1824*, 246–252.

Kuznetsov, N.A., Koval, V.V., Nevinsky, G.A., Douglas, K.T., Zharkov, D.O., and Fedorova, O.S. (2007). Kinetic conformational analysis of human 8-oxoguanine-DNA glycosylase. J. Biol. Chem. *282*, 1029–1038.

Lazareno-Saez, C., Arutyunova, E., Coquelle, N., and Lemieux, M.J. (2013). Domain swapping in the cytoplasmic domain of the *Escherichia coli* rhomboid protease. J. Mol. Biol. *425*, 1127–1142.

Lemberg, M.K., and Freeman, M. (2007). Functional and evolutionary implications of enhanced genomic analysis of rhomboid intramembrane proteases. Genome Res. *17*, 1634–1646.

Li, X., Wang, B., Feng, L., Kang, H., Qi, Y., Wang, J., and Shi, Y. (2009). Cleavage of RseA by RseP requires a carboxyl-terminal hydrophobic amino acid following DegS cleavage. Proc. Natl. Acad. Sci. USA *106*, 14837–14842.

Li, X., Dang, S., Yan, C., Gong, X., Wang, J., and Shi, Y. (2013). Structure of a presenilin family intramembrane aspartate protease. Nature *493*, 56–61.

López-Otín, C., and Bond, J.S. (2008). Proteases: multifunctional enzymes in life and disease. J. Biol. Chem. *283*, 30433–30437.

Makinoshima, H., and Glickman, M.S. (2006). Site-2 proteases in prokaryotes: regulated intramembrane proteolysis expands to microbial pathogenesis. Microbes Infect. *8*, 1882–1888.

Moin, S.M., and Urban, S. (2012). Membrane immersion allows rhomboid proteases to achieve specificity by reading transmembrane segment dynamics. Elife *1*, e00173.

Osenkowski, P., Ye, W., Wang, R., Wolfe, M.S., and Selkoe, D.J. (2008). Direct and potent regulation of gamma-secretase by its lipid microenvironment. J. Biol. Chem. *283*, 22529–22540.

Perona, J.J., and Craik, C.S. (1997). Evolutionary divergence of substrate specificity within the chymotrypsin-like serine protease fold. J. Biol. Chem. *272*, 29987–29990.

Rather, P.N., Ding, X., Baca-DeLancey, R.R., and Siddiqui, S. (1999). *Providencia stuartii* genes activated by cell-to-cell signaling and identification of a gene required for production or activity of an extracellular factor. J. Bacteriol. *181*, 7185–7191.

Schnaitman, C.A. (1970a). Examination of the protein composition of the cell envelope of *Escherichia coli* by polyacrylamide gel electrophoresis. J. Bacteriol. *104*, 882–889.

Schnaitman, C.A. (1970b). Protein composition of the cell wall and cytoplasmic membrane of *Escherichia coli*. J. Bacteriol. *104*, 890–901.

Shah, S., Lee, S.F., Tabuchi, K., Hao, Y.H., Yu, C., LaPlant, Q., Ball, H., Dann, C.E., 3rd, Südhof, T., and Yu, G. (2005). Nicastrin functions as a gamma-secretase-substrate receptor. Cell *122*, 435–447.

Stennicke, H.R., Renatus, M., Meldal, M., and Salvesen, G.S. (2000). Internally quenched fluorescent peptide substrates disclose the subsite preferences of human caspases 1, 3, 6, 7 and 8. Biochem. J. *350*, 563–568.

Stevenson, L.G., Strisovsky, K., Clemmer, K.M., Bhatt, S., Freeman, M., and Rather, P.N. (2007). Rhomboid protease AarA mediates quorum-sensing in *Providencia stuartii* by activating TatA of the twin-arginine translocase. Proc. Natl. Acad. Sci. USA *104*, 1003–1008.

Strisovsky, K., Sharpe, H.J., and Freeman, M. (2009). Sequence-specific intramembrane proteolysis: identification of a recognition motif in rhomboid substrates. Mol. Cell *36*, 1048–1059.

Timmer, J.C., Zhu, W., Pop, C., Regan, T., Snipas, S.J., Eroshkin, A.M., Riedl, S.J., and Salvesen, G.S. (2009). Structural and kinetic determinants of protease substrates. Nat. Struct. Mol. Biol. *16*, 1101–1108.

Urban, S. (2009). Making the cut: central roles of intramembrane proteolysis in pathogenic microorganisms. Nat. Rev. Microbiol. *7*, 411–423.

Urban, S. (2010). Taking the plunge: integrating structural, enzymatic and computational insights into a unified model for membrane-immersed rhomboid proteolysis. Biochem. J. *425*, 501–512.

Urban, S., and Wolfe, M.S. (2005). Reconstitution of intramembrane proteolysis in vitro reveals that pure rhomboid is sufficient for catalysis and specificity. Proc. Natl. Acad. Sci. USA *102*, 1883–1888.

Urban, S., and Baker, R.P. (2008). In vivo analysis reveals substrate-gating mutants of a rhomboid intramembrane protease display increased activity in living cells. Biol. Chem. *389*, 1107–1115.

Urban, S., and Dickey, S.W. (2011). The rhomboid protease family: a decade of progress on function and mechanism. Genome Biol. *12*, 231.

Vinothkumar, K.R., Strisovsky, K., Andreeva, A., Christova, Y., Verhelst, S., and Freeman, M. (2010). The structural basis for catalysis and substrate specificity of a rhomboid protease. EMBO J. *29*, 3797–3809.

Wilderman, P.J., Vasil, A.I., Martin, W.E., Murphy, R.C., and Vasil, M.L. (2002). *Pseudomonas aeruginosa* synthesizes phosphatidylcholine by use of the phosphatidylcholine synthase pathway. J. Bacteriol. *184*, 4792–4799.

Wolfe, M.S. (2009). Intramembrane proteolysis. Chem. Rev. *109*, 1599–1612.

Wysocka, M., Lesner, A., Legowska, A., Jaśkiewicz, A., Miecznikowska, H., and Rolka, K. (2008). Designing of substrates and inhibitors of bovine alpha-chymotrypsin with synthetic phenylalanine analogues in position P(1). Protein Pept. Lett. *15*, 260–264.

Xue, Y., and Ha, Y. (2012). Catalytic mechanism of rhomboid protease GlpG probed by 3,4-dichloroisocoumarin and diisopropyl fluorophosphonate. J. Biol. Chem. *287*, 3099–3107.

Xue, Y., Chowdhury, S., Liu, X., Akiyama, Y., Ellman, J., and Ha, Y. (2012). Conformational change in rhomboid protease GlpG induced by inhibitor binding to its S' subsites. Biochemistry *51*, 3723–3731.

Zhang, D., and Kovach, I.M. (2006). Deuterium solvent isotope effect and proton-inventory studies of factor Xa-catalyzed reactions. Biochemistry *45*, 14175–14182.

Zhou, Y., Moin, S.M., Urban, S., and Zhang, Y. (2012). An internal water-retention site in the rhomboid intramembrane protease GlpG ensures catalytic efficiency. Structure *20*, 1255–1263.

Cell

EXTENDED EXPERIMENTAL PROCEDURES

DNA Cloning

Rhomboid proteases were cloned by PCR amplification from purified genomic DNA (ATCC) with primers encoding a single N-terminal HA-tag. All constructs were verified by sequencing the entire ORF.

Thermostability Analysis

HA-*Ec*GlpG was preincubated at pH 4 with 10 mM NaAcetate, 150 mM NaCl, 0.1% DDM or pH 7 with 50 mM Tris pH 7.4, 150 mM NaCl, 0.1% DDM for 1 hr at room temperature, after which the proteins were neutralized with 7 volumes of 50 mM Tris pH 7.4, 150 mM NaCl, 0.1% DDM. Thermostability was assayed as previously described (Baker and Urban, 2012) using a Stargazer-384 instrument (Harbinger Biotech).

Rhomboid Protease Crystallization and Structure Determination

ΔN-GlpG from *E. coli* was expressed and purified as described previously (Wu et al., 2006), and crystallized in hanging drops at pH 4.5 in 0.1 M Na-Acetate, 3 M NaCl and 10% glycerol and at pH 7.5 in 0.1 M HEPES, 3 M NaCl and 10% Glycerol at room temperature. Crystals were cryo-protected in a reservoir buffer containing 15% (v/v) Glycerol and flash-frozen in a nitrogen stream. X-ray diffraction data were collected at F1 station of the Cornell High Energy Synchrotron Source (CHESS), and processed using HKL2000 (Otwinowski and Minor, 1997). The structures were solved by molecular replacement using coordinates of native GlpG (PDB 2IC8) as the probe with the program MOLREP in the CCP4 program suite (Collaborative Computational Project, Number 4, 1994). Initial refinement was performed using CNS (Brünger et al., 1998) with positional, simulated annealing, and individual temperature factor refinement protocols. Model building was carried out iteratively in *coot* (Emsley and Cowtan, 2004) based on σ_A-weighted $2F_o - F_c$ and $F_o - F_c$ maps. After CNS refinement converged, further refinement was conducted with REFMAC5 (Murshudov et al., 2011). The final model for both GlpG structures contained residues 91–272.

CysTatA-His Cleavage Assay

CysTatA-His (expressed from pET27b as residues 1-33 of 97 with a C-terminal poly6-His fusion and a cysteine inserted after the start codon) was purified using a Ni^{2+} affinity resin (Roche), concentrated to ~500 μM and dialyzed against 50 mM Tris, 150 mM NaCl, 0.2% sarkosyl, and 1 mM DTT. Purified CysTatA-His was reconstituted as described into *E. coli* lipids with either HA-*Ec*GlpG WT or the catalytic mutant HA-*Ec*GlpG S201A+H254A. Reactions were incubated at 37°C and time points of each reaction were quenched with SDS-sample buffer. Samples were resolved on a 16% polyacrylamide, 6 M urea, SDS, tricine gel at 120 V for 2 hr. After transfer to a nitrocellulose membrane, the membrane was probed with a mouse anti-His-647 direct conjugated antibody (QIAGEN) and imaged with an Odyssey infrared scanner.

Mass Spectrometry of FITC-TatA Cleavage

FITC-TatA cleaved in proteoliposomes was filtered through a 30,000 MW cutoff centrifugal filter (Millipore) following the manufacturer's protocol. The sample was purified using a C18 ZipTip (Millipore), and analyzed by MALDI-TOF using a Voyager DE-STR mass spectrometer calibrated with bradykinin fragment 1-7, angiotensin I, ACTH fragment 18-39, and insulin oxidized B chain (Sigma-Aldrich).

FITC-TatA Labeling and Orientation

400 pmoles of FITC-TatA, containing a single cysteine at the C terminus, were reconstituted into *E. coli* lipids to 0.5 mole%. Following ultracentrifugation, membrane pellets were resuspended with 50 mM Tris pH 7.4, 150 mM NaCl with or without 0.2% sarkosyl. DMSO or 4 μmoles of the membrane-impermeable IR800cw-maleimide dye (Li-Cor Biosciences) was added to each sample as indicated and incubated at room temperature for 2 hr to label exposed cysteines. Labeling was quenched by adding 1,000 μmoles of DTT and incubating for 30 min. Samples were resolved by SDS-PAGE and imaged with an Odyssey infrared scanner (Li-Cor Biosciences) in both the 700 and 800 channels.

Active Site Labeling

Purified rhomboid proteases were labeled with the activity-based isocoumarin inhibitor JLK6 (Tocris Biosciences) to determine the fraction of purified protein that was active. Rhomboid protein in 50 mM Tris pH 7.4, 150 mM NaCl, 0.1% DDM was incubated with either 10% DMSO only or carrying 400 μM JLK6 at 37°C for 3 hr, purified using a C4 ZipTip, and analyzed by mass spectrometry as described previously (Pierrat et al., 2011).

FRET Analysis of Protease-Substrate Affinity in Membranes

Purified N-terminally His-tagged *Ec*GlpG H254A+C104A+W196C protein was labeled at the single cysteine residue with the FRET acceptor tetramethylrhodamine-5-maleimide (TMR) (Life Technologies). Reconstitutions into *E. coli* liposomes were performed as described above, except that 30 pmoles of TMR-labeled protein was mixed with 25 – 800 pmoles of the FITC-TatA ligand. Following reconstitution, the samples were incubated at 37°C in a Synergy H4 Hybrid plate reader. Fluorescence was measured with excitation

at 485 nm and emission from 510 – 600 nm in 5 nm intervals. The FRET interaction was calculated at the 580 nm emission wavelength by subtracting the TMR-labeled GlpG protein alone and the FITC-TatA alone samples from the sample containing both macromolecules.

Proteolysis Assays in Detergent Micelles

Cleavage reactions of APP+Spi7-Flag were performed as described previously and imaged with an Odyssey infrared scanner (Li-Cor Biosciences) (Baker and Urban, 2012; Baker et al., 2007). The kinetics of FITC-TatA cleavage were examined under different conditions and in various detergents before settling on the following optimized protocol: FITC-TatA in 50 mM Tris pH 7.4, 150 mM NaCl, 1 mM DTT, 0.15% Sarkosyl, 0.1% (w/v) DDM was preincubated at 37°C for 10 min, centrifuged at 13,000 rpm in a microcentrifuge for 10 min to remove any insoluble substrate, and mixed with 83 nM HA-*Ec*GlpG in reaction tubes prewarmed to 37°C. Reactions were quenched and analyzed on 16% tricine gels as above. Actual substrate concentrations were calibrated using FITC-TatA standards analyzed in parallel.

Coprecipitation Analysis

2.5 μM His-tagged *Ec*GlpG C104A+H254A with 70 μM FITC-TatA was incubated with pre-equilibrated Ni^{2+}-NTA resin (QIAGEN) for 3 hr at room temperature. The resin was washed, and bound proteins were eluted with SDS-sample buffer for 30 min. FITC-TatA was detected as above using a 16% Tricine gel and a Typhoon Imager. His-*Ec*GlpG C104A+H254A was detected by western blot with the mouse anti-penta−His antibody (QIAGEN), and imaged with an Odyssey infrared scanner (Li-Cor Biosciences).

HPLC Equilibrium Gel Filtration Analysis

Two Superdex 200 PC 3.2/30 high-resolution gel filtration columns (GE Healthcare) were connected in tandem to a ProStar 410 HPLC system (Agilent/Varian), and equilibrated with 9.5 μM FITC-TatA in 2 mM phosphate buffer pH 7.4, 25 mM Tris pH 7.4, 120 mM NaCl, 0.15% Sarkosyl, 0.1% DDM, 1 mM DTT. 20 μM HA-*Ec*GlpG S201A+H254A was preincubated with 9.5 μM FITC-TatA, and 50 μl was injected using an Autosampler 410 onto the columns at a flow rate of 0.05 ml/minute. Elution was monitored by absorbance at all wavelengths between 200 to 600 nm simultaneously using a PDA 330 detector. The FITC-TatA peak was quantified relative to known FITC-TatA concentration standards that were run on the columns equilibrated with 9.5 μM FITC alone in buffer. Conventional gel filtration was conducted under similar conditions, except the columns were equilibrated with buffer lacking FITC-TatA.

Chromosomal Engineering of *E. coli*

Allelic exchange "knock-in" of the *E. coli* chromosomal *glpG* gene was achieved by two successive rounds of homologous recombination using standard recombineering methods (Datsenko and Wanner, 2000). In the first round, the entire *glpG* gene was replaced in BW25113 Str^R cells via homologous flanking ends with a cassette that encodes a selection and a counter-selection marker (*cat-rpsL*: chloramphenicol acetyltransferase [*cat*] and wild-type *rpsL* to confer resistance to chloramphenicol and sensitivity to streptomycin, respectively) by selecting for growth in the presence of 17.5 μg/ml chloramphenicol. In the second round, the now chromosomally encoded cassette was replaced with either a Flag or hemagglutinin epitope tag fused to the 5′ end of the *glpG* DNA sequence (Flag-GlpG or HA-GlpG) using the same flanking homology ends by counter-selecting for the desired strain for growth in the presence of 200 μg/ml streptomycin. The resulting strains, Flag-GlpG and HA-GlpG, were confirmed by PCR and sequencing.

SUPPLEMENTAL REFERENCES

Brünger, A.T., Adams, P.D., Clore, G.M., DeLano, W.L., Gros, P., Grosse-Kunstleve, R.W., Jiang, J.S., Kuszewski, J., Nilges, M., Pannu, N.S., et al. (1998). Crystallography & NMR system: a new software suite for macromolecular structure determination. Acta Crystallogr. D Biol. Crystallogr. *54*, 905–921.

Collaborative Computational Project, Number 4 (1994). The CCP4 suite: programs for protein crystallography. Acta Crystallogr. D Biol. Crystallogr. *50*, 760–763.

Datsenko, K.A., and Wanner, B.L. (2000). One-step inactivation of chromosomal genes in *Escherichia coli* K-12 using PCR products. Proc. Natl. Acad. Sci. USA *97*, 6640–6645.

Emsley, P., and Cowtan, K. (2004). Coot: model-building tools for molecular graphics. Acta Crystallogr. D Biol. Crystallogr. *60*, 2126–2132.

Murshudov, G.N., Skubák, P., Lebedev, A.A., Pannu, N.S., Steiner, R.A., Nicholls, R.A., Winn, M.D., Long, F., and Vagin, A.A. (2011). REFMAC5 for the refinement of macromolecular crystal structures. Acta Crystallogr. D Biol. Crystallogr. *67*, 355–367.

Otwinowski, Z., and Minor, W. (1997). Processing of X-ray diffraction data collected in oscillation mode. Methods Enzymol. *276*, 307–326.

Pierrat, O.A., Strisovsky, K., Christova, Y., Large, J., Ansell, K., Bouloc, N., Smiljanic, E., and Freeman, M. (2011). Monocyclic β-lactams are selective, mechanism-based inhibitors of rhomboid intramembrane proteases. ACS Chem. Biol. *6*, 325–335.

Wu, Z., Yan, N., Feng, L., Oberstein, A., Yan, H., Baker, R.P., Gu, L., Jeffrey, P.D., Urban, S., and Shi, Y. (2006). Structural analysis of a rhomboid family intramembrane protease reveals a gating mechanism for substrate entry. Nat. Struct. Mol. Biol. *13*, 1084–1091.

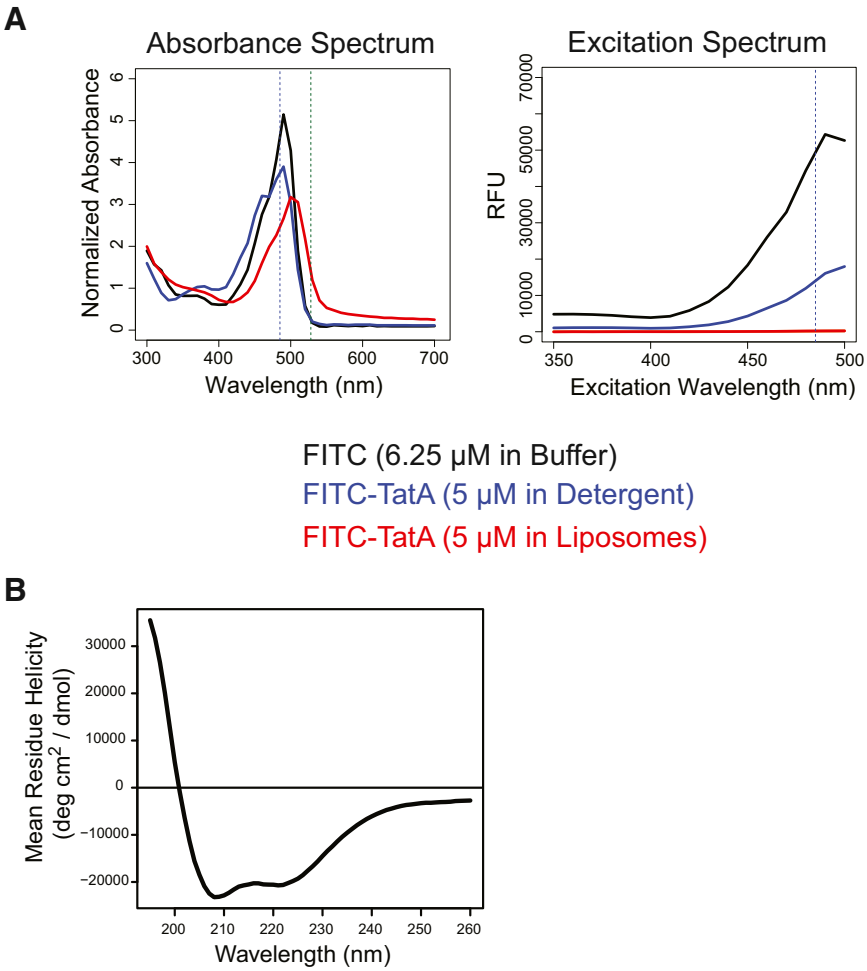

Figure S1. Spectral Evaluation of the FITC-TatA Substrate, Related to Figure 2

(A) Fluorescence of FITC-TatA was quenched in proteoliposomes (red), but not in detergent micelles (blue). FITC-TatA in proteoliposomes maintained the ability to absorb (left panel), but failed to fluoresce over a range of excitation and emission wavelengths (blue dashed line = 485 nm, green dashed line = 528 nm).

(B) Circular dichroism analysis of FITC-TatA reconstituted in *E. coli* lipids showed that FITC-TatA adopts a helical secondary structure.

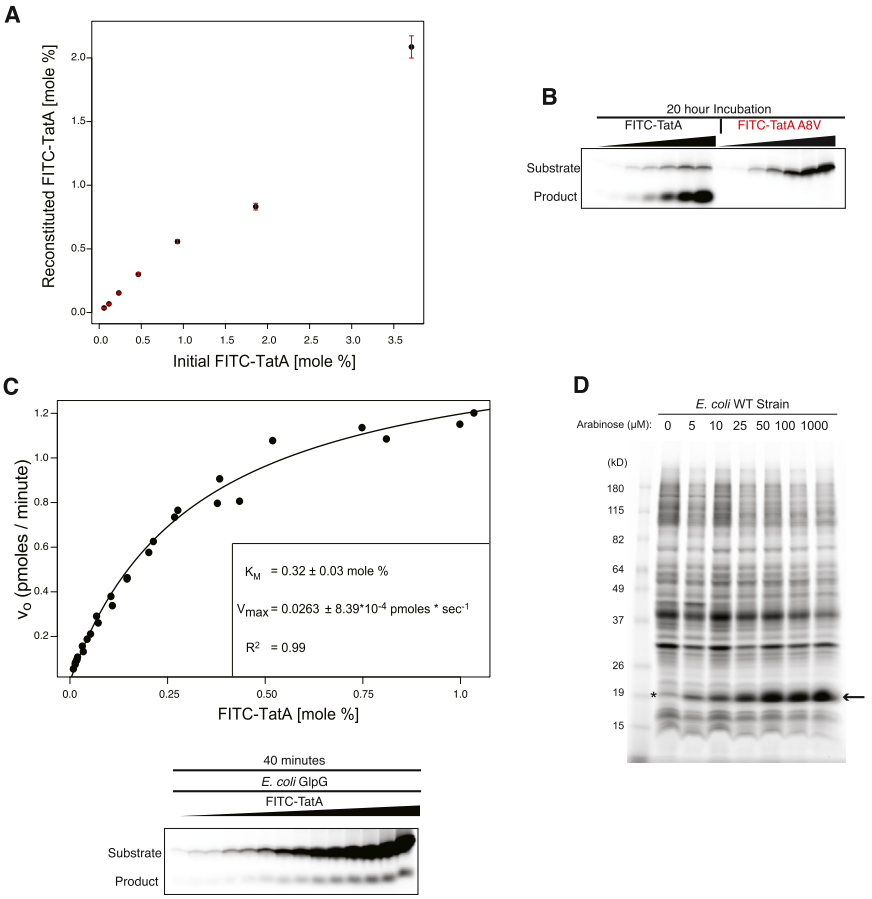

Figure S2. Further Characterization of TatA Reconstitution and Proteolysis, Related to Figure 3

(A) Reconstitution efficiency of FITC-TatA into proteoliposomes quantified by fluorescence was consistent (mean ± SEM, n = 14).

(B) Extended incubation of FITC-TatA cleavage with HA-*Ec*GlpG revealed the majority of substrate was turned over. Shown is a fluorescence scan of a 16% tricine gel.

(C) A Michaelis-Menten (inset: fit ± SD) model fitted to data derived from a 40 min reaction of HA-*Ec*GlpG cleavage of FITC-TatA analyzed by SDS-PAGE on a 16% tricine gel (lower image). No cooperativity was observed in the gel-analyzed fit.

(D) Coomassie stained gel of titrated TatA-Flag membrane preparations. TatA-Flag (arrow) accumulates to ~20% of all membrane proteins. The asterisk denotes a background band comigrating with TatA-Flag, the signal of which was subtracted from the TatA-Flag signal.

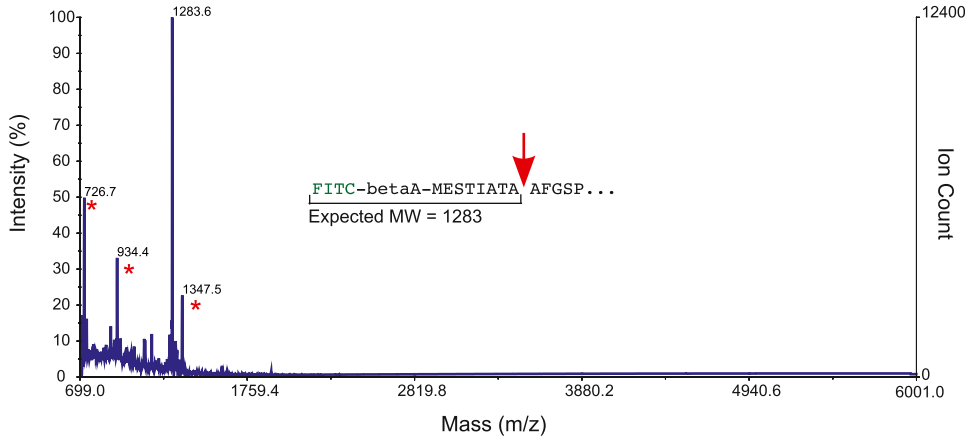

Figure S3. Additional Cleavage Site Analysis, Related to Figure 5

MALDI-TOF mass spectral analysis of the FITC-TatA cleavage product generated by the gate-open mutant *Ec*GlpG F153A+W236A. Red asterisks denote background peaks that correspond to no predicted mass/charge ratio of other potential cleavage sites. These are likely to be carryover lipid species.

A

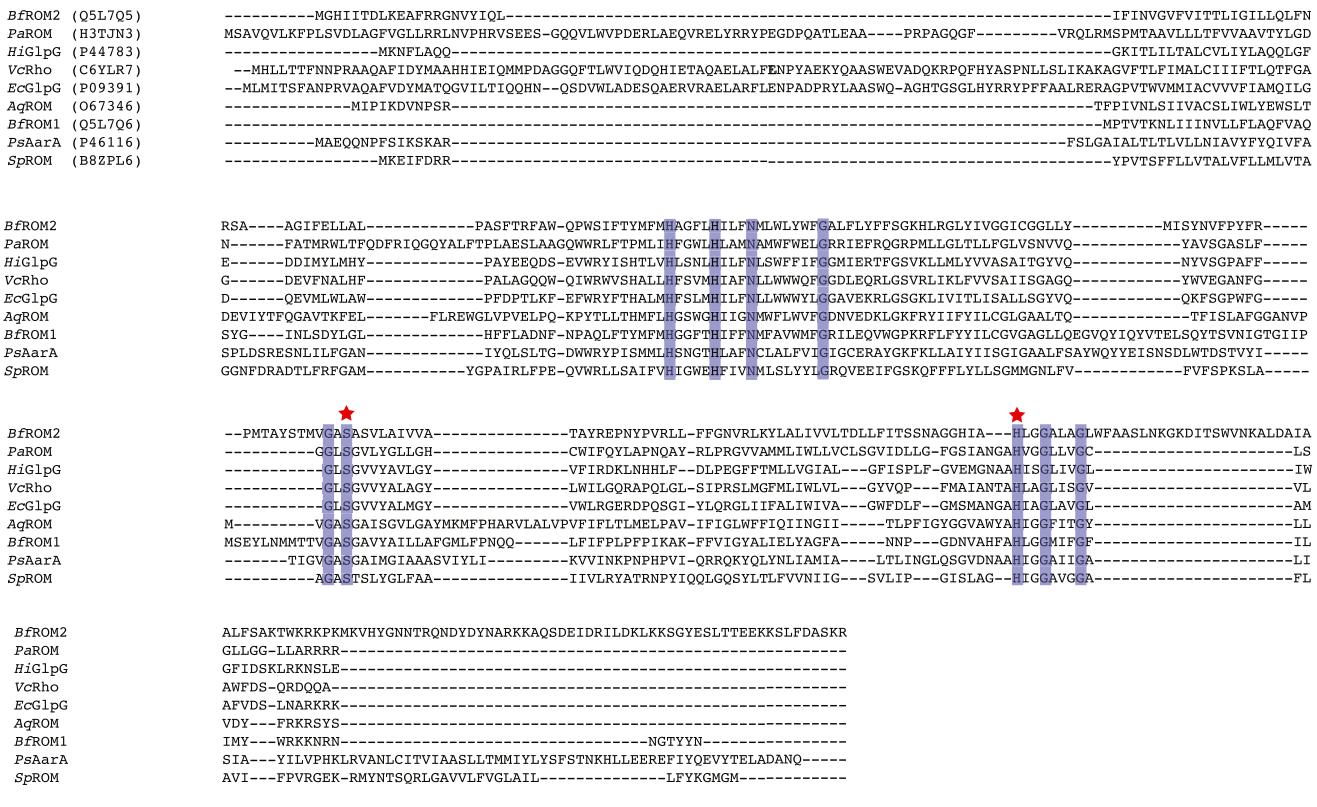

B

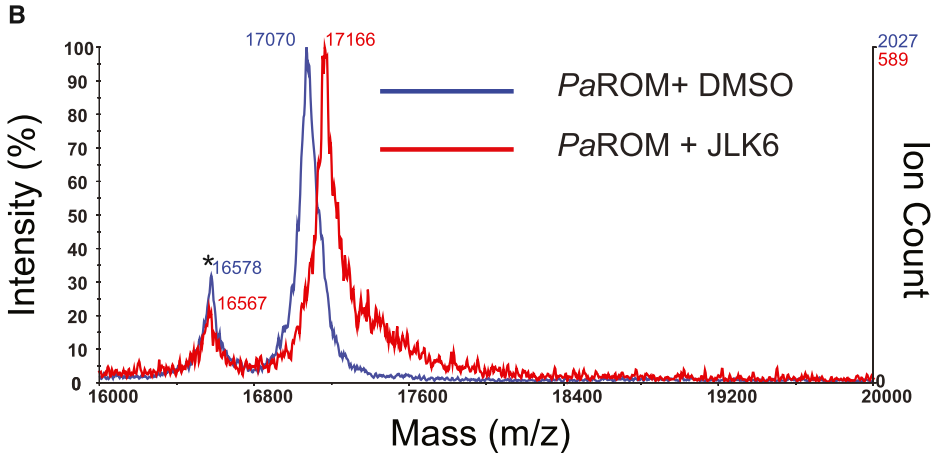

Figure S4. Analysis of Diverse Rhomboid Enzymes, Related to Figure 6

(A) MUSCLE multiple sequence alignment of the 9 rhomboid proteases analyzed. Universally conserved residues are shaded in blue, and red stars denote active site serine and histidine residues. UNIPROT accession numbers are in parentheses.

(B) Mass spectrum of *Pa*ROM, the slowest rhomboid analyzed, incubated with the activity-based inhibitor JLK6 revealed our enzyme preparations to be 100% active. Shown is the doubly-charged species. The asterisk denotes a background peak, which served as an internal control for the overlaid mass spectra.

Table S1. Crystallographic Statistics, Related to Figure 1

	GlpG-pH7.5	GlpG-pH4.5
Data collection		
Space group	*R32*	*R32*
Unit cell dimensions		
a, *b*, *c* (Å)	110.6, 110.6, 127.7	110.7, 110.7, 127.8
α, β, γ (˚)	90, 90, 120	90, 90, 120
Resolution (Å)	50.0–2.17 (2.21-2.17) [a]	50.0–2.28 (2.32-2.28)[a]
Observations	103,835	107,735
Unique reflections[a]	29,338 (952)	26,208 (1617)
Redundancy	3.5 (1.6)	4.1 (3.3)
$I/\sigma I$	13.8 (1.9)	8.3 (2.2)
Completeness (%)[a]	99.5 (62.5)	99.7 (70.6)
R_{merge} (%)[a,b]	6.2 (54.2)	11.5 (55.3)
Refinement		
Resolution (Å)	50.0–2.4 (2.46-2.40) [a]	44.9–2.4 (2.46-2.40) [a]
No. of reflections	9,925	9,029
R_{work} / R_{free}	0.187 / 0.244 (0.179/0.282) [a]	0.198 / 0.248 (0.259/0.292) [a]
No. of atoms	1502	1502
Protein residues	1452	1452
Water molecules	50	50
Average *B* factors (Å^2)	43.5	47.5
Protein	43.2	44.6
Water	53.4	49.9
RMSD		
Bonds (Å)	0.017	0.018
Angles (˚)	1.75	1.97

[a]Values in parentheses correspond to highest resolution shell. [b]$R_{merge} = (\Sigma|I(i) - \langle I(h)\rangle|/ \Sigma I(i))$. [c]$R_{work} = \Sigma|F_o - F_c|/\Sigma F_o$. [d]$R_{free}$ was calculated over reflections in a test set not included in atomic refinement: GlpG-pH7.5, 4.9%; GlpG-pH4.5, 5.0%.